



# Multi-scale analysis of the influence of physicochemical parameters on the hydrodynamic and gas-liquid mass transfer in gas/liquid/solid reactors

A. Kherbeche, J. Milnes, Mélanie Jimenez, Nicolas Dietrich, Gilles Hébrard,  
B. Lekhlif

## ► To cite this version:

A. Kherbeche, J. Milnes, Mélanie Jimenez, Nicolas Dietrich, Gilles Hébrard, et al.. Multi-scale analysis of the influence of physicochemical parameters on the hydrodynamic and gas-liquid mass transfer in gas/liquid/solid reactors. Chemical Engineering Science, 2013, 100, pp.515 - 528. 10.1016/j.ces.2013.06.025 . hal-01268234

**HAL Id: hal-01268234**

**<https://hal.science/hal-01268234>**

Submitted on 18 Jul 2021

**HAL** is a multi-disciplinary open access archive for the deposit and dissemination of scientific research documents, whether they are published or not. The documents may come from teaching and research institutions in France or abroad, or from public or private research centers.

L'archive ouverte pluridisciplinaire **HAL**, est destinée au dépôt et à la diffusion de documents scientifiques de niveau recherche, publiés ou non, émanant des établissements d'enseignement et de recherche français ou étrangers, des laboratoires publics ou privés.

**MULTI-SCALE ANALYSIS OF THE INFLUENCE OF PHYSICOCHEMICAL  
PARAMETERS ON THE HYDRODYNAMIC AND GAS-LIQUID MASS  
TRANSFER IN GAS/LIQUID/SOLID REACTORS**

A. Kherbeche <sup>a,b,c,d,e</sup>, J. Milnes <sup>c,d,e</sup>, M. Jimenez <sup>c,d,e</sup>, N. Dietrich <sup>c,d,e,\*</sup>, G. Hébrard <sup>c,d,e</sup>, B. Lekhlif <sup>a,b</sup>

<sup>a</sup> Environmental Engineering Laboratory of EHTP , Hassan II University, Morocco

<sup>b</sup> Polymer research team, ENSEM, Hassan II University, Morocco

<sup>c</sup> Université de Toulouse; INSA,UPS,INP; LISBP, 135 Avenue de Rangueil, F-31077

Toulouse, France

<sup>d</sup> INRA, UMR792, Ingénierie des Systèmes Biologiques et des Procédés, F-31400

Toulouse, France

<sup>e</sup> CNRS, UMR5504, F-31400 Toulouse, France

\* Corresponding Author: Nicolas Dietrich

E-mail: Nicolas.Dietrich@insa-toulouse.fr

## 26    **Abstract**

27    The present paper reports an original, predominantly experimental study of the mass  
28    transfer efficiency in biofilters. Hydrodynamic and mass transfer parameters were  
29    investigated at two different scales. These parameters have been first considered (i) at a  
30    global scale in a three-phase fixed bed reactor with investigating the influence of the  
31    physic chemical properties of liquid phase and then (ii) from a local point of view by  
32    focusing at the bubble/packing contact. Experiments at global scale have been conducted  
33    in a semi-industrial scaled reactor (4.5 m height, 0.15 m in diameter) operating in batch  
34    mode, in co-current gas-liquid upflow. Air was injected at the bottom of the reactor  
35    through porous disc diffusers. Two kinds of packing, Meteor and Biolite, which have  
36    been thoroughly studied by Maldonado et al. (2008), have been tested and compared. The  
37    impact of the liquid phase was investigated for different solutions containing clear water  
38    and some additives (salts, sugar, suspended solids and varied pH) that can be encountered  
39    in industry. For each liquid phase tested, gas holdup, pressure drop, slip velocities and  
40    bubble sizes were estimated, as well as volumetric mass transfer coefficients under  
41    different superficial gas velocities (ranging from  $2.3 \cdot 10^{-3} \text{ m.s}^{-1}$  to  $2.9 \cdot 10^{-2} \text{ m.s}^{-1}$ ). For all  
42    the tested cases, variations in the hydrodynamic behavior were observed with increasing  
43    superficial gas velocity and with all the compounds added to the liquid phase. Mass  
44    transfer coefficients decreased with all the tested compounds except for low  
45    concentrations of salts, acid and basic solution. Local-scale experiments were performed  
46    in a 2D cell made of *PMMA*, with a height of 200 mm, width of 100 mm and thickness  
47    of 2 mm, to investigate the visualization of mass transfer and hydrodynamics in the axial  
48    profile of bubbles rising through a fixed bed. A high speed camera was used with an  
49    oxygen sensitive dye to visualize oxygen transfer and Kalliroscope particles to visualize

bubble hydrodynamics. A specific approach was proposed for estimating the mass transfer coefficient in such a configuration. It was found that the mass transfer coefficient  $k_L$  depended on bubble behavior through the packing. Low porosity of packing, bubble size and velocity were the principal parameters influencing the hydrodynamics and mass transfer coefficients at this scale.

This study considered a new approach to obtain precise data on biofilter systems, investigate the hydrodynamics and gas-liquid mass transfer at two scales, enriching the database on biofilters and providing new insights that could improve this system in industry.

**Keywords:** Hydrodynamics, Mass transfer coefficient, Complex media, Bubbles, Visualization.

## 1. Introduction

Usually called biofilters, fixed bed reactors are mainly used for carbon, nitrogen and suspended particle elimination in the aerobic treatment of urban wastewaters. Today they have several applications in industry (Indrani 2005; Chaudhary 2003). In wastewater treatment, biofilters combine compactness and high removal efficiencies. These gas/liquid/solid systems, in presence of pollutants, develop a fixed biomass clinging to the solid phase to purify wastewater. Bacterial activity for wastewater treatment in the biofilter involves several steps (Gullicks et al., 2011), each of which induces a variation in the physicochemical quality of the liquid phase, sometimes limiting performance or, in more critical cases, leading to malfunction.

It is well known that the hydrodynamics and gas-liquid mass transfer in bioreactors, where the gas is the dispersed phase, play a key role in the performance of such systems. This performance depends on the amount of oxygen that aeration systems are able to supply to the bacteria that are attached to the fixed packing. Therefore, it is necessary to investigate the effect that variations in the physicochemical quality of the liquid phase during bacterial activity has on the hydrodynamics and mass transfer and to monitor their incidence on the performance of the biofilter.

Characterizing hydrodynamics and mass transfer in the presence of biomass or real wastewater is delicate because of the complex nature of such media. As a first approach, it seems thus interesting to consider clear water and suspensions of known constituents that may give a physicochemical quality similar to that of wastewater. Such synthetic media should mainly be composed of salts, organic matter, different kinds of suspended solids and considered at different ranges of pH, and thus viscosities. However even when considering this simplified configuration, difficulties to characterize such systems are

many-sided since hydrodynamics and mass transfer are directly linked to numerous parameters such as liquid phase properties, characteristics of the bed, gas injection system, etc. In literature, it has been shown for instance that the gas holdup and pressure drop in packed bubble columns depend on the way the three phases are present in the system. Sundararajan and Ju (1993) explained that hydrodynamics and mass transfer were influenced by three factors:

1- Changes of the chemical medium properties by the cells activity,

2- Presence of solid particles,

3- Mass transfer enhancement by the reaction. Maldonado et al. (2008), Daeosong Ju et al. (2008a, 2011b), and Bhatia et al. (2004) have shown the effect of physical properties of the solid phase. The introduction of a solid phase as a fixed bed in a bubble column affects the size of the bubbles and their behavior. The first parameters that can influence this behavior are the porosity of the packing, the particle diameters and particle density.

Many authors have shown that the gas holdup and the volumetric oxygen mass transfer coefficient increase with the superficial air velocity (Maldonado et al.; 2008). The diffuser also has considerable importance for conditioning the hydrodynamics and mass transfer. Hébrard et al. (1996) found that spargers generating small bubbles were the best for promoting mass transfer as their interfacial area was large. Concerning impacts of the liquid composition, several studies focused on diphasic systems. For instance, Jamongwong et al. (2010) treated the effect of salts on a small scale, finding that they affected the size of bubbles and changed their physical interface characteristics, thus modifying the mass transfer by minimizing coalescence phenomena. Studies have also shown the increase of gas holdup when salts are present (Hikita et al., 1974). The

addition of organic compounds in the liquid phase is not without effect. Plais et al. (2005) and Dumont et al. (2006) have shown that adding an organic phase dispersed in an aqueous phase decreases the mass transfer. Jamongwong et al. (2010) also tested the effect of glucose in a diphasic system, showing that it decreased the liquid side mass transfer coefficient  $k_L$ . The addition of solid micro-particles decreases the volumetric mass transfer coefficient and also the gas holdup in a diphasic system, as was shown by Plais et al. (2005). Omota et al. (2006) studied the effect of the behavior of several types of solid particles (based on carbon and silicate) in gas bubbles. They were shown to affect the way in which the bubble transferred oxygen, in particular that the lower part of the bubble was where oxygen passed to the next stage in the case of with two phases. Lopez-Lopez et al. (2007) found that the pH did not greatly influence the mass transfer or the hydrodynamics, and the viscosity of the liquid phase increased gas holdup and decreased the volumetric mass transfer coefficient by reducing the diffusion coefficient of oxygen in the liquid (Stemmet et al., 2008).

However, such studies are scarce when considering threephasic systems. The purpose of this paper is thus to compare these conclusions to those obtained in a semi-industrial scaled reactor. Impacts of packing, liquid composition and gas superficial velocity on hydrodynamics and mass transfer have been obtained, analyzed and presented in this paper.

But it can be note that when considering this global approach, the behavior between bubbles and packing, which is of prime interest when dealing with mass transfer efficiencies, is delicate to quantify. A second set of experiments have thus been conducted to locally and directly visualize hydrodynamics and mass transfer behaviors in

the wake of single air bubbles rising in presence of packing in a simplified 2D Hele-Shaw cell. In the literature, some researchers investigated colorimetric techniques by means of an oxygen or dioxygen carbon sensitive dyes but this approach is very delicate and difficult. In this paper, Two original and promising techniques, colorimetric (for mass transfer) and Kallirosopic (for hydrodynamics) techniques, are developed in this paper to achieve such interesting visualizations in such type of reactors. Based on these visualizations, a comparison in terms of mass transfer efficiency has been performed for two kinds of packing and for different packing orders.

By considering global and local experiments, a new and original approach is proposed to go beyond the understanding of the different mechanisms operating in gas/liquid/solid systems.

.



## 2. Materials and Methods

As mentioned in the introduction, experiments to study the hydrodynamics and mass transfer were carried out on two scales. An almost industrial scale with large dimensions was used to observe the phenomena of hydrodynamics and mass transfer generally and, in parallel, local scale experiments, with dimensions similar to those of the particles of the packing, were performed to search for more precise explanations of the results found at the global scale.

### 2.1 Global Scale

At the global scale, the experiments were carried out in a fixed-bed column 4.5 m high and 0.15 m in diameter made of transparent PVC. Water and gas were introduced at the bottom of the column. Whatever the operating conditions, the water regime was discontinuous (batch mode) (Figure 1). Two kinds of packing, Meteor and Biolite, were tested and filled the column to a height of 3.5 m. Their physical properties, presented in Table 1, have been studied by Garcia Maldonado (2007).

The packing was fixed using a grid. It has been observed that pressure drop caused by the grid was negligible. The liquid phase flow was steady and its physicochemical quality was varied, the concentrations of compounds being chosen among values encountered in the wastewater treatment industry. In the experiments, clear water was used with the addition of some compounds. Thus, the influence of sodium chloride was examined for a range of 1 to 10 g.L<sup>-1</sup>, then the concentration of glucose was varied from 0 to 50 g.L<sup>-1</sup>. The influence of suspended matter was investigated using the effect of two products, a clay (bentonite) for concentrations of 0.1 to 1 g.L<sup>-1</sup>, and suspended carbonaceous

174 material (Acticarbon or powdered coal) at 0.1 to 1 g.L<sup>-1</sup>. The effect of pH was studied  
 175 using sodium hydroxide, NaOH, for basic pH and sulfuric acid, H<sub>2</sub>SO<sub>4</sub>, for acid pH.  
 176 Compressed air was used to inject gas into the column with a porous sparger. The  
 177 bubbles leaving the diffuser were between 2 and 6 mm in diameter (Hébrard et al.; 1996)  
 178 the superficial velocity of air was varying from 2.3 10<sup>-3</sup> to 2.9 10<sup>-2</sup> m.s<sup>-1</sup> in the column.  
 179 The behavior of bubbles inside the column and through the packing were observed with a  
 180 high speed camera (Photron SA3), located in the middle of the column at a height of 2.2  
 181 m. Images were taken at 500 frames per second. The window is 50mm×50mm.

182 The liquid phase was introduced using a peristaltic pump, filling slowly to drive out any  
 183 air bubbles that might have become trapped between packing particles. In all the  
 184 experiments, the initial liquid height was kept constant at 3.8 m. Next, the air was  
 185 injected. The gas holdup is the volume of gas in the column compared to the total volume  
 186 after injection of the gas (Eq.1). In other words, the gas holdup is the difference of water  
 187 level observed in the liquid phase before and after gas injection. The volume of gas  
 188 retained in the liquid segment is equal to the volume of water displaced and can be  
 189 calculated by the following formula (Eq.2):

$$\mathcal{E}_G = \frac{V_G}{V_T} \quad (1)$$

190

$$\mathcal{E}_G = \frac{(D_c^2)(h - h_0) + (h_{\text{surv}})(D_{\text{surv}}^2 - D_c^2) - 4(U_G)(D_c^2)(h - h_0)}{(D_c^2)(H_B)} \quad (2)$$

191

For the pressure drop determination, pressure taps were installed along the height of the column, at 0.2m, 2m and 3.5 m from the bottom, and were connected to a U tube.

Once the column had been filled with the liquid phase, the oxygen was almost completely stripped from the water by injection of pure nitrogen at very high flow rate through the distributor. A calibrated Mettler-Toledo sensor placed at the top of the column at 3.8 m height showed a value of 0 mg.L<sup>-1</sup> at the beginning of the experiments (Figure 1). Air was then sparged into the column and the oxygen was taken up by the liquid phase. The total measurement time was chosen long enough for the oxygen saturation concentration  $C^*$  to be reached (about 15 min, a measurement each 5 seconds), the rising curve following the relation (Eq.3):

$$\ln \frac{C^* - C}{C^* - C_0} = -k_L a \cdot t \quad (3)$$

The interfacial area depends on the bubble size and is given by Equation 4: (According to the study of Garcia Maldonado *et al.* (2008),  $\varepsilon_s$  was given for each packing used)

$$a = \frac{6}{d_b} \cdot \frac{\varepsilon_G}{1 - \varepsilon_G - \varepsilon_s} \quad (4)$$

Based on high-speed camera acquisitions, bubble diameters,  $d_b$ , were easily determined using Equation (5).

$$d_b = (h_b l_b^2)^{1/3} \quad (5)$$

(6)

$$d_{bm} = \frac{\sum_m (d_b^3)}{\sum_m (d_b^2)}$$

207 The average number of bubbles measured was about 200 per configuration. The behavior  
208 of bubbles was analyzed and the number of occasions when bubbles coalesced or broke  
209 up was calculated in each configuration.

210 The liquid side volumetric mass transfer coefficient  $k_L$  was calculated by means of the  
211 volumetric mass transfer coefficient  $k_{La}$  found in the experiments and the interfacial area.

## 212 2.2 Local scale

213 Several 2D-packed configurations (called packed channel) were created to represent the  
214 3D fixed bed in order to visualize how the bubble hydrodynamics could impact the mass  
215 transfer and what the influence of the nature/shape of the packing was. These systems  
216 were adapted in a Hele-Shaw cell (0.1×0.1 m visualization chamber made of transparent  
217 PMMA (PolyMethylMethAcrylate) with a very small depth of 0.002 m) and the particles  
218 were packed vertically to produce a vertical channel for the bubble injected at an orifice  
219 at the bottom of the cell (see Figure 2). The size of the bubble was chosen to be around  
220 2.5 mm in order to represent the bubble size in biofilters. Four different distances  $D$   
221 between particles lines were tested with Meteor (2, 5, 8 and 10 mm) and three with  
222 Biolite (2, 4, and 6 mm). A high speed camera was placed in front of the cell, with a  
223 shutter speed of 1/1000 s, an acquisition rate of 2000 frames/second.

224 The purpose of this local approach is to observe the hydrodynamics and mass transfer  
225 behaviors in the wake of rising bubbles in the configuration presented above just by using  
226 a high-speed camera. Two visualization techniques have thus been tested: a colorimetric

one for visualizing mass transfer and another with Kalliroscope particles for the hydrodynamics.

### 2.3 Kalliroscope technique

The local hydrodynamics, which also affects bubble behavior in the packing, was studied by means of a virtual rheoscopic fluid (VRF) called Kalliroscope (Matisse and Gorman, 1984). This product is a liquid additive (Andereck et al., 1986) which contains microscopic reflective flakes that orient themselves with bubble flow in 2D cells. The flakes are strongly reflective in some areas and nearly transparent in others which allow a direct visualization of the hydrodynamics behavior in the bubble path. For these experiments a solution with 50% w/w of Kalliroscope in demineralized water has been considered. An example of visualization performed using these particles is presented in Figure 11-a. It can be note that this technique has been used just to visualize the hydrodynamics behavior in the bubble path in order to compare it with mass transfer. No quantification purposes have been considered.

### 2.3 Colorimetric technique

The colorimetric technique is based on the use of an oxygen-sensitive dye. Its main advantage is that it is non-intrusive, as the measurements are carried out without disturbing the flow or inserting a physical sensor. There are a large number of organic chemical compounds that present the following properties when subjected to an oxidation/reduction reaction:

- intense color in the oxidized or reduced state
- no color or a different color in the conjugate (opposite) state.

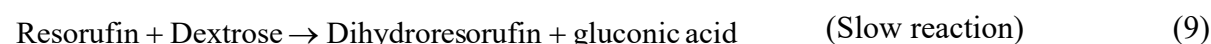
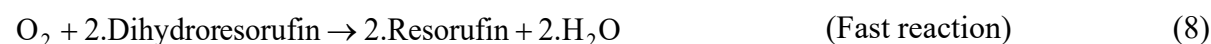
For example, methylene blue is blue in the oxidized state but colorless in the reduced state. The well-known “blue bottle” experiments use this property (Cook et al., 1994; Walter et al, 1997; Engerer and Cook, 1999; Wellman and Noble, 2003).

In this study, several dyes were tested: methylene blue, indigo carmine and resazurin. Resazurin was finally chosen because it gave a good compromise between speed of the kinetics and color to be achieved. In addition, resazurin is well known as its reduction has been used for about 50 years to monitor bacterial and yeast contamination of milk, and also for assessing semen quality (O’Brien et al, 2000).

As shown in Figure 3, resazurin (blue and not fluorescent) is reduced into resorufin (pink and highly fluorescent), which is itself reduced to dihydroresorufin (colorless and not fluorescent). These reactions are catalyzed by the presence of glucose and sodium hydroxide. In alkaline solutions, glucose is oxidized to D-gluconic acid or alpha-D-gluconolactone:



The change of color results from the reversible oxidation-reduction reactions between resorufin (pink) and dihydroresorufin (colorless):



Note that the complete chemical formula of resazurin is 7-Hydroxy-3H-phenoxazin-3-one-10-oxide (molecular mass 229.19 g.mol<sup>-1</sup>).

272

273 A preliminary study (not detailed here) was carried out to define the best composition of  
274 the catalyst (glucose and sodium hydroxide) in the dye solution, i.e. the one leading to:

- 275 - (quasi)-instantaneous kinetics for the oxidation of dihydroresorufin (colorless)  
276 into resorufin (pink),
- 277 - sufficiently slow kinetics (few minutes) for the reduction of resorufin (pink)  
278 into dihydroresorufin (colorless),
- 279 - high colorimetric yield (i.e. the color intensity).

280

281 From this, the following formulation was chosen: glucose and sodium hydroxide were  
282 both diluted at  $20 \text{ g.L}^{-1}$  in deionized water, and the concentration of resazurin was fixed  
283 at  $0.1 \text{ g.L}^{-1}$ .

284 Based on this technique and just by using a high-speed camera, the mass transferred in  
285 the bubble wake could easily be visualized since a darker area appeared on the recorded  
286 image (darker area representing the pink form of the dye and thus the presence in  
287 oxygen). An example of such a visualization is proposed in Figure 4-a.

288

## 289 2.4 Image processing

290 Based on this kind of images (Figure 4-a), a specific approach has been developed to  
291 quantify this mass transferred in the bubble wake to compare efficiencies for the different  
292 tested configurations. To achieve this quantification, the first step was to establish a  
293 calibration curve between the “grey level” observed on the recorded image and the  
294 corresponding oxygen concentration. For this, several colorimetric solutions were  
295 prepared at different concentrations of resazurin ( $0.05$  and  $0.01 \text{ g.L}^{-1}$ ). They were

saturated in oxygen with air in order to reach their highest intensity of pink (or their highest value of grey level on the acquired image). For each colorimetric solution flowing in the cell (without bubbles), about 50 pictures were recorded and averaged. In addition, images were acquired when no oxygen was present in the colorimetric solution. The third averaged images obtained showed how the grey level changed according to the resazurin concentration (Figure (5-b)).

The stoichiometry of the reaction between oxygen and dihydroresorufin is given by Equation 8. Then, the number of moles of dissolved oxygen can easily be deduced from the number of moles of resazurin, as

$$n_{O_2 transferred} = n_{O_2 reacted} = \frac{n_{dihydroresorufin}}{2} = \frac{n_{resazurin}}{2} \quad (10)$$

Thus, for each resazurin concentration (0, 0.05 and 0.1 g.L<sup>-1</sup>), it was possible to associate the observed averaged grey level with a dissolved oxygen concentration. The calibration curve obtained is plotted in Figure 5-a. The perfect linearity observed between grey level and dissolved oxygen concentration is remarkable and is an undeniable advantage of this method. It is also important to note that this calibration curve is attached to the present experimental set-up and conditions. In other words, if a change was made in the light or camera parameters, the calibration would have to be performed again. Based on this calibration curve, grey levels recorded by the camera could thus be converted into oxygen concentration. However further efforts have to be considered before achieving accurate quantification. A specific image processing, whose only the basic principles are presented in this paper, has thus been developed. An example of raw image to be corrected is depicted in Figure 4-a. As a first step, an image reference is subtracted to the raw image. This reference image is an image without any bubble or mass transfer. By subtracting these two images, packing and impurities on the picture have been removed (see Figure



4-b). However due to some temporal non-homogeneities of the lighting, the background grey level (and oxygen concentration) could differ from 0. The background grey level had thus to be set to 0 to not alter mass transfer calculations. On the resulting image (See Figure 4-c), only remain the bubble and its mass transferred. Bubble edges have been detected using specific algorithms (Canny edge detector, extracted from Image Processing Toolbox in Matlab®). Bubbles edges have thus been detected (Figure 4-d) and removed (Figure 4-e) from the corresponding image. Figure 4-e represents an example of corrected image where non null pixels represented a certain amount of oxygen transferred by the bubble. The total amount of mass transferred could easily be determined by considering the estimated concentration pixel per pixel.

### 3. Results at global scale

The results of the gas holdup experiments are reported as a function of gas velocity in Fig. 7. It is clear that, whatever the type of solid, the gas holdup increases with increasing superficial gas velocity  $U_G$ , for all the liquid phases tested. Gas holdup was also found to depend on physical characteristics of the packing, such as the apparent porosity, particle size (as was shown by Garcia Maldonado (2007)). For a packing of low porosity, breakup occurs and no large bubbles form, (Moustiri et al.; 2002). Thus the contact area between particles and bubbles is large (Maldonado et al.; 2008). The reduction induced in the slip velocity therefore increases the gas holdup. This is shown in Figure 7-b, where gas holdup values reported for Biolite range between 0.04 and 0.07, while the values for Meteor are between 0.01 and 0.05, the range of superficial gas velocity  $U_G$  being from 0.0023 m.s<sup>-1</sup> to 0.0117 m.s<sup>-1</sup> in both cases.

Concerning the influence of the physicochemical properties of the liquid phase, as shown in Figures 7-a, 7-b and 7-c, it is clear that, for Meteor, the addition of salts (from 1 to 10 g.L<sup>-1</sup>) increases the gas holdup from 0.017 to 0.064 for the same gas flow rates ( $U_G = 0.0023 \text{ m.s}^{-1}$ ) and from 0.067 to 0.128 for high gas flow rates ( $U_G = 0.029 \text{ m.s}^{-1}$ ). Salt addition acts on the bubble behavior by causing an increase in the surface tension and viscosity of the liquid (Jamongwong et al.; 2010). Then, numerous small static bubbles were observed to be embedded between packing particles (see section 2) due to the high surface tension, which reduced the coalescence, especially for high concentrations of salts. It was also noted that the way gas holdup increased with salt concentration depended on the type of packing for the same gas superficial velocity. In fact, figure 7-c shows that the rate of increase of gas holdup for Biolite was lower than that observed in Meteor.

The addition of glucose did not have any great effect on gas hold-up. In Fig7-c, it is clear that gas holdup tends to stabilize at high concentrations of glucose (10 to 50 g.L<sup>-1</sup>): with  $U_G = 0.0023 \text{ m/s}$ , it does not exceed 0.026 for the Meteor and 0.048 for the Biolite. Adding glucose decreased the surface tension of the liquid and this was the principle cause of a small decrease in the gas hold up even for higher concentrations with the same superficial gas velocity.

The suspended solid micro particles added to the liquid phase increased the gas holdup smoothly, as illustrated in figures 7-a and 7-b. Increasing the concentration of bentonite from 0.3 to 1 g.L<sup>-1</sup> decreased gas holdup from 0.023 to 0.017. Explanations have been given for the micro scale by Omota et al. (2006), who used coal powder with the liquid and gas. They considered the contact area of the small particles used but did not give results concerning the direct effect of the presence of these particles on gas holdup. The

effect of coal powder (Acticarbon) on gas holdup was the same in the present work. Gas holdup varied from 0.02 to 0.014 for concentrations ranging from 0.3 to 1 g.L<sup>-1</sup>. Finally, the pH did not have a marked effect on gas holdup; the difference of values with pure water did not exceed 0.3% but gas holdup with an acidic liquid phase was slightly less than for the basic liquid phase.

The pressure drop measured at the top of the column in our experiments increased due to the increase in gas superficial velocities. Pressure drops for Meteor varied from 0.8 % to 8 % when superficial velocity varied from 0.0023 to 0.029 m.s<sup>-1</sup> whereas, for Biolite, it ranged between 1 % and 10 %. Bed porosity, contact area and particle shape factor were the parameters that most influenced pressure drop. Increasing doses of salts and glucose increased the pressure drop by about 1 % and 5 % relative to clean water. The suspended solid micro particles increased the pressure drop by about 4 % for bentonite and 0.5 % for Acticarbon.

Due to increasing gas holdup, the slip velocity decreased with increasing gas superficial velocity.

$$G = \frac{U_G}{\varepsilon_G} \quad (11)$$

Generally, slip velocities in experiments carried out on Biolite were lower than on Meteor (Table 3) because the low porosity bed led to high gas holdup and low slip velocities. The bubbles could be assumed to be broken by interaction with the wire of the packing and the large density of small, uniform-sized bubbles was maintained. The higher values of gas holdup and the uniform bubble size can explain the decrease in slip velocity in the presence of packing. With high doses of salts (10 g.L<sup>-1</sup>) and thus increased surface

tension, small bubbles became more rigid and led to high values of gas holdup. This explains the decrease of almost 10% in slip velocity in the presence of salts. However, for glucose (50 g.L<sup>-1</sup>), slip velocity decreased due the increase in the viscosity of the liquid by almost 8 % in Meteor. Suspended solids did not strongly influence slip velocity because of the low concentrations of bentonite and coal powder used in the experiments.

Experiments showed that the interfacial area calculated from equation (4) increased with the superficial gas velocity (Fig. 8-a) for all liquid phases under test. The interfacial area results are shown as a function of gas velocity in Fig. 8. The interfacial area depends on the bubble diameter and it has also been shown that the influence of the solid phase is critical to bubble diameter and behavior. In fact, within the Meteor bed it was observed that the bubbles in the column were composed of three populations (Fig.6-a). The first kind of bubble encountered was small bubbles, not exceeding 2 mm, clinging to the static packing. Even at high superficial gas velocity, these bubbles became static, mainly when the surface tension of liquid phase was strong, as with highest concentrations of salts. Small bubbles were rigid and fixed in the packing. These kinds of bubbles, also influenced by the porosity of the packing and the particle shapes, were at the origin of the gas holdup results. The second population of bubbles had sizes between 2 and 6 mm, which were generally dynamic. Variations in the liquid characteristics influenced this population. The third population was composed of large bubbles (air pockets) of sizes greater than 6 mm, which were always moving through the bed, sometimes taking small bubbles with them. Their average behavior was usually determined by the bed porosity and the physicochemical quality of the liquid phase, and also by the superficial gas velocity.

411 Compared to Meteor, the bubbles observed in Biolite (Fig.6-b) were always the same.  
412 Bubbles were seen to be constantly in movement, mainly because of the very low  
413 porosity of Biolite. The contact time between bubbles and packing was long, thus  
414 encouraging coalescence among bubbles moving in the packing. It was found that  
415 interfacial area on Meteor was higher than that found on Biolite (Fig 8-b).

416 Concerning the superficial gas velocity effect, it was found that increasing superficial gas  
417 velocities increased interfacial area, a result also reported by Maldonado (2007), Bhatia  
418 (2004) and Moustiri (2002) (Fig. 8-a, 8-b).

419 The study of the effect of the physicochemistry of the liquid phase revealed that, in  
420 different salt concentrations (from 1 to 10 g.L<sup>-1</sup>) for the case of Meteor, it was difficult to  
421 see the calculated difference in bubble sizes. The average did not change, so it was hard  
422 to say that bubble size changed with concentration of salts. On the other hand, it is  
423 possible that the salinity influenced bubble surface characteristics indirectly by changing  
424 the coalescence rate between bubbles. A low concentration of salts would make bubble  
425 surfaces more favorable to coalescence, while high concentrations of salts would lead to  
426 small, more rigid bubbles and increase the attachment of these bubbles to the particles of  
427 packing, thus giving the biggest gas holdup in the experiments. The number of small,  
428 static bubbles for a concentration of 1 g.L<sup>-1</sup> of salt was 8% whereas for 10 g.L<sup>-1</sup>, their  
429 number rose to 35%, which explains the reduction of coalescence phenomena as the  
430 interfacial area was then largest (Fig 8-c). Concerning added glucose, it must have  
431 changed the liquid viscosity, mainly for high concentrations (from 10 to 50 g.L<sup>-1</sup>). In this  
432 interval, bubble sizes in Meteor were found to be slightly smaller, and the average varied  
433 from 3.32 to 2.32 mm with a superficial gas velocity  $U_G = 0.0023 \text{ m.s}^{-1}$ . Glucose acted  
434 indirectly on the surface of bubbles by reducing the liquid viscosity. Bubbles were then

smaller and the interfacial area larger. Suspended solids have a key effect on the surface of bubbles, which depends on the nature of the suspended solids added. In our case, for bentonite, the processed images showed that bubble sizes changed, decreasing from 2.63 mm to 2.35 mm for Meteor. For coal, the bubble sizes decreased from 2.19 mm to 1.93 mm, but this was not observed for Biolite. It is important to mention that Omota et al., (2006) found that coal powder could be spread around the bubble and limit the transfer, mainly in the zone beneath the bubble. The pH did not have any great influence on bubble size.

The results concerning the volumetric mass transfer coefficient  $k_La$  in Figure 9 show that increasing superficial gas velocity increases  $k_La$ . The same result has been found in many works concerning tri-phasic systems (Maldonado (2007), Bhatia (2004) and Moustiri (2002)). The effect of the solid phase is crucial in mass transfer. Values of  $k_La$  with Biolite were slightly higher than for the Meteor in this work (Fig.9.b). The gas holdup, which influences the interfacial area, gave values of  $k_La$  between 0.0013 and 0.0151  $s^{-1}$  for Biolite. These values were always higher than those for Meteor, which gave values between 0.0013 and 0.0128  $s^{-1}$  in the range of superficial gas velocity between 0.0023 and 0.0029  $m.s^{-1}$ . The hydraulic regime was strongly influenced by the nature of the solid. There was little difference between  $k_La$  for low flows whereas, for high flow rates, differences could reach 0.002  $s^{-1}$ .

The physicochemical quality of the liquid phase influenced the mass transfer coefficient obtained for a constant gas flow ( $U_G = 0.0023 m.s^{-1}$ ). Up to 10  $g.L^{-1}$  for Meteor (Fig.9-c), the salt addition increased the mass transfer to 0.0028  $s^{-1}$  and, with a maximum of 5  $g.L^{-1}$  for Biolite, it also reached 0.0028  $s^{-1}$ . For higher salt concentrations (10 to 50  $g.L^{-1}$ ), the mass transfer coefficient decreased dramatically. The trends observed previously for the

behavior of bubbles confirm the findings for mass transfer evolution: the phenomena of coalescence and breakup were present and the transfer was greater when superficial gas velocities were large. As noted previously, salts acted on the surface of bubbles. At low concentrations (less than 10 g.L<sup>-1</sup>), oxygen transfer was higher because the bubble surfaces became more active, and that explains the higher  $k_{La}$  found. High concentrations of salt induced an increase in the liquid surface tension, allowing smaller and more rigid bubbles to become embedded among packing particles.

The effect of glucose on the mass transfer was negative. For low concentrations of glucose, the mass transfer coefficient increased to 0.0026 s<sup>-1</sup> for Meteor and 0.0025 s<sup>-1</sup> for Biolite. Then, beyond a certain concentration, mass transfer was observed to drop until it reached 0.0016 s<sup>-1</sup>. It has been seen that the interfacial area was larger and coalescence and breakup were lower for both packed beds. Adding glucose enhanced the viscosity of the liquid phase, thus allowing a decrease in slip velocity that could explain these values of  $k_{La}$ . Jamongwong et al. (2010) studied the effect of glucose on the liquid side mass transfer coefficient and found that glucose decreased  $k_{La}$  in the small scale gas/liquid system. Asgharpour et al. (2010), and Bhatia et al. (2004) found that the effect of organic solvents and contaminants influenced the mass transfer coefficient negatively. Results were the same for both gas/liquid and gas/liquid/solid column reactors.

$k_{La}$  was negatively influenced by the presence of suspended solids. Bentonite decreased  $k_{La}$  from 0.0022 s<sup>-1</sup> for a null bentonite concentration  $C_B = 0$  g.L<sup>-1</sup> to 0.0019 s<sup>-1</sup> for  $C_B = 1$  g.L<sup>-1</sup>, while coal had a dramatic effect on transfer values up to 0.0013 s<sup>-1</sup> at  $C_B = 1$  g.L<sup>-1</sup>. Omota (2006) observed the negative effect of suspended solids on the adhesion of solid micro-particles to the gas. In our case, the packing acted as a block for suspended solids and this could promote streaking of coal micro-particles on the surface of bubbles. This

may have limited the phenomena at the interface of the bubble and may have decreased the gas / liquid mass transfer. It was also shown that the coal (Acticarbon) decreased the transfer more than bentonite did (Fig.9-a). The effect of pH did not influence the transfer greatly: it was found that with a pH of 9.79, there was a slight decrease in  $k_{La}$ , 1% compared to that of water (pH = 7.56), while at pH 3.5, there was an increase of 1% in  $k_{La}$ .

It was found that the liquid side mass transfer coefficient increased when slip velocities were higher and allowing higher slip velocity could increase  $k_L$ . This result confirms Maldonado et al.'s findings calculated values of  $k_L$  encountered for Biolite were slightly higher than those found in Meteor (Table 3). It was also found that, for lower concentrations of salt and glucose,  $k_L$  increased by 80 % for both types of packing for the same superficial gas velocity ( $U_G = 0.0023 \text{ m.s}^{-1}$ ) and it decreased by about 60% for high concentrations. Bentonite and Acticarbon both increased the  $k_L$  by about 40 % but, for higher concentrations, it was found that  $k_L$  decreased. This was due to the interfacial area calculated with the real bubble size encountered in each experiment.

#### **4. Results at local scale**

First experiments conducted for this local approach were based on the hydrodynamics behavior in the bubble wake for different spaces  $D$  between particles (Figure 2) using Kalliroscope particles. It was observed that, without packing particles, bubbles (2.5 mm diameter, velocity of 0.188 m/s.) followed a zigzag path, leaving a Karman vortex street in their wake (Fig 10.a). Adding particles laterally to the bubble injection did not affect the hydrodynamic structure until a distance between particles of about 10 mm was reached, where the trajectories were clearly impacted as shown in figure 10-b. It was



observed that a distance greater than three times the bubble diameter was not interesting for visualizing an impact of the packing.

It has been observed that in presence of Meteor particles, the bubble tended to oscillate strongly between particles (Fig 11-a) in comparison with the absence of packing (Fig 10-a). These perturbations in the wake of the bubbles were also visible in the colorimetric technique raw images (Fig 11-b). The observations on the mass transferred by the bubble confirm the experiment on hydrodynamics using the Kallirosopic particles mentioned above. Oscillating rising was also observed and this movement was also present in the bubble wake; the oxygen concentration field followed the streamline. Image processing using Matlab® software calculated the total amount of oxygen dissolved in the wake of the bubble as:

$$\overline{m} = \iiint C(x, y).dx \cdot dy \cdot dz \quad (12)$$

These values and the bubble properties (size, velocity) are reported in table 4. As observed in figure 11-b, more than ten times as much oxygen was transferred for the 2-mm channel ( $3.85 \times 10^{-8}$  mg) as the 10-mm channel ( $1.65 \times 10^{-9}$  mg). This difference could be explained by the smaller bubble velocity in the 2-mm channel and by the impact of the packing geometry, which increased the agitation in the wake, renewing the bubble surface. In contrast, Biolite particles are nearly circular, and this caused a disturbance but not with the same intensity as for Meteor (Fig 11-a). The amount of oxygen was also smaller, ranging from  $2.54 \times 10^{-8}$  mg for the 2-mm channel to  $8.03 \times 10^{-9}$  for the 6-mm channel (Table 4).

The shape of the packing bed played a key role. More oxygen was transferred with Meteor than with Biolite for the same channel diameter. This may have been due to the

velocity of the bubbles, observed to be higher in Biolite than in Meteor, changing the contact time of the bubble in the cell. The kalliросcopic technique, by providing the hydrodynamic structure, confirmed that the wake structure for Meteor led to a better mixing in the channel, improving the efficiency of the transfer. These experiments showed the important contribution made by the packing in a biofilter; the filter particles characterized the movement and behavior of bubbles within the biofilter, which influenced the mass transfer inside the system.

The purpose of this final section is to evaluate the liquid-side mass transfer coefficient ( $k_L$ ) from the dissolved oxygen concentration fields presented above (Fig 5.).

As established by Roudet et al. (2011), the volumetric mass flux of oxygen from gas to liquid along a channel can be expressed as:

$$\varphi(X') = u_B \cdot \frac{\partial \bar{C}}{\partial X'} \quad (13)$$

where  $X'$  is the axial position in the channel such that  $X' = 0$  at the location where the bubbles are generated and  $X' = 0.2$  m at the exit of the channel.  $\bar{C}$  is the average concentration in dissolved oxygen accumulated in the channel (mainly in the bubble wake) at the axial position  $X'$  along the vertical channel. Assuming that the concentration of dissolved oxygen in the liquid at the scale of the unit cell is zero due to its consumption by the chemical reaction, the mass flux of oxygen (per unit of liquid volume) can also be expressed by:

$$\varphi(X') = k_L \cdot a \cdot C^* \quad (14)$$

549 where  $k_L$  is the liquid-side mass transfer coefficient,  $a$  the interfacial area between gas  
 550 and liquid phases and  $C^*$  the dissolved oxygen saturation concentration ( $C \sim 8 \text{ mgL}^{-1}$ ).

551 By coupling Equations 13 and 14, relationship 15 is found:

$$552 \quad \frac{\partial \bar{C}}{\partial X'} = \frac{k_L \cdot a \cdot C^*}{u_B} \quad (15)$$

553 If the oxygen transferred at the bubble formation is neglected, integrating Equation 15  
 554 over the entire cell gives:

$$555 \quad \bar{C} = \frac{k_L \cdot a \cdot X' \cdot C^*}{u_B} \quad (16)$$

556 In order to estimate the interfacial area,  $a$ , between the gas and liquid phases, a  
 557 cylindrical shape is assumed for a bubble between the two walls. This is true only for  
 558 bubbles having diameters bigger than the thickness of the cell (i.e. 2 mm in our case).

559 With these assumptions, the specific interfacial area for the liquid film  $a$  is given by:

$$560 \quad a = \frac{\pi \cdot d_B \cdot e}{V_{channel}} = \frac{\pi \cdot d_B}{X' \cdot D} \quad (17)$$

561 The order of magnitude of the interfacial area,  $a$ , goes from 50 to 500  $\text{m}^2 \cdot \text{m}^{-3}$ . As  
 562 expected (Yue et al, 2007), the values of  $a$  are significantly higher than in usual gas–  
 563 liquid macro-contactors such as our global scale experiments. They are almost the same  
 564 as in static mixers and smaller than in microchannels.

565 The oxygen transferred by a single bubble can then be tracked by the dissolved oxygen  
 566 accumulation in the cell, as:

$$\bar{C} = \frac{\bar{m}}{V_{channel}} = \frac{\iiint C(x, y).dx \cdot dy \cdot dz}{X.D.e} \quad (18)$$

Equation 18 does not take the dimension  $z$ , related to the channel width, into account for integrating  $C$ . This is because the present colorimetric technique is not able to discriminate the visualizations at different planes along the channel width. Consequently, we should keep in mind that the oxygen concentration fields visualized are the result of all the different fields existing at all the vertical locations.

Finally, from Equations 16 and 17, the liquid-side mass transfer coefficient can be calculated as:

$$k_L = \frac{\bar{C} \times u_B}{X' \times a \times C^*} \quad (19)$$

The variation of  $k_L$  with gas flow rate is plotted in figure 13 (the associated numerical values being reported in Table 4). A decrease in the mass transfer coefficient is observed with an increase in particle distance. This decrease is attributable to the decrease in the slip bubble velocity.

In order to validate the colorimetric technique, the liquid-side mass transfer coefficients above should be compared to those found in the literature and especially with the liquid-side mass transfer coefficients from Higbie's penetration theory as:

$$k_L = 2 \sqrt{\frac{D}{\pi \cdot t_C}} \quad (20)$$

585 Rather good agreement with Higbie's model is observed ( $\sim 3 \times 10^{-5}$  m/s), demonstrating  
586 how this new visualization technique (easy to implement as without a laser source) can  
587 bring new insights for investigating mass transfer processes in a packed bed. Although  
588 some experimental aspects remain to be perfected, these original results provide new  
589 insight into a theoretical model and numerical simulation.

590

#### 4. Conclusion

The effect of the physicochemical composition of the liquid phase on hydrodynamics and gas-liquid mass transfer was studied on two scales: a bubble packed-bed column on global scale and a Hele Shaw cell on a local scale. On the global scale, clean water was used with addition of some compounds like salts, sugar, pH modifying compounds, and suspended solids. Several measurement techniques were employed to obtain a good characterization of the hydrodynamic parameters and mass transfer characteristics under various operating conditions. Two kinds of packing were used. Superficial gas velocity was varied in the range of  $2.3 \cdot 10^{-3} \text{ m.s}^{-1}$  to  $2.9 \cdot 10^{-3} \text{ m.s}^{-1}$ . It was found that the physicochemical properties of the liquid phase, the superficial gas velocity and the physical characteristics of the solid phase all had an effect on hydrodynamics and mass transfer.

- The increase in superficial gas velocity increased gas holdup and mass transfer coefficient. An increase was also observed in the interfacial area, which was independent of the quality of liquid or solid phase in the biofilter.
- High concentrations of salts increased gas holdup, decreased bubble size and thus increased interfacial area. The mass transfer coefficient increased up to a concentration of  $10 \text{ g.L}^{-1}$  and then decreased dramatically.
- Glucose had a slight impact on gas holdup. It was shown that, with high concentrations of glucose, gas holdup increased a little.. Both superficial area and mass transfer decreased with glucose.

- Two kinds of suspended solids were used, bentonite and Acticarbon. They increased gas holdup but decreased the mass transfer coefficient. Acticarbon was shown to have more effect on mass transfer than bentonite.

- pH did not have a big impact on hydrodynamics. Gas hold up and interfacial area were shown to stay stable for acidic and basic pH. It was found that mass transfer increased with pH.

To gain insight into this extraordinary complexity involving hydrodynamics, mass transfer, and interfacial phenomena, some preliminary results were obtained within a 2D-device by means of a newly developed technique. These new experimental results prefigure some possibilities to develop and validate modeling and simulations. At this scale, it has been shown that the oxygen transferred depends on the porosity of the packing, and the arrangement of packing particles. It also depends on the bubble-packing contact time. The present study has clearly highlighted the need to complete the database related to oxygen diffusion coefficients in biofilters. It can give more information about how to improve water and wastewater treatment efficiencies.

This study thus constitutes a striking example showing that this new colorimetric method could be an interesting tool for investigating gas-liquid mass transfer in transparent fluids, with a view to reactor design. This information gives new insight into the complex mechanism of bubble mass transfer and could help to develop rigorous theoretical models and numerical simulations.

635    **Acknowledgement**

636    This study was supported by the United Nations Educational, Scientific and Cultural  
637    Organization – UNESCO for young researchers in the Water Science Domain.

638



$a$	<i>Interfacial area (<math>m^{-1}</math>)</i>
$C$	<i>Dissolved oxygen concentration at time <math>t</math> (<math>g.l^{-1}</math>)</i>
$C^*$	<i>Dissolved oxygen saturation concentration (<math>g.l^{-1}</math>)</i>
$C_i$	<i>Concentration of compounds (<math>g.l^{-1}</math>)</i>
$D$	<i>Distance between two particles lines in the Hele-Shaw cell = channel size (<math>m</math>)</i>
$d_b$	<i>Single Bubble diameter (<math>mm</math>)</i>
$d_{bm}$	<i>Mean bubble diameter (<math>mm</math>)</i>
$D_c$	<i>Column diameter (<math>m</math>)</i>
$D_{surv}$	<i>Overflow column diameter (<math>m</math>)</i>
$e$	<i>Hele-Shaw cell thickness (<math>m</math>)</i>
$G$	<i>Slip velocity (<math>m.s^{-1}</math>)</i>
$h$	<i>Height of water after gas injection (<math>m</math>)</i>
$h_0$	<i>Height of water before gas injection (<math>m</math>)</i>
$H_B$	<i>Bed height (<math>H_B</math>) (<math>m</math>)</i>
$h_b$	<i>Height of bubble (<math>mm</math>)</i>
$H_L$	<i>Liquid height (<math>m</math>)</i>
$h_{surv}$	<i>Height of water on overflow (<math>m</math>)</i>
$H_T$	<i>Total height (<math>m</math>)</i>
$k_L$	<i>Liquid-side mass transfer coefficient (<math>m.s^{-1}</math>)</i>
$k_{L,a}$	<i>Volumetric mass transfer coefficient (<math>s^{-1}</math>)</i>
$l_b$	<i>Width of bubble (<math>mm</math>)</i>
$PMMA$	<i>PolyMethylMethAcrylate</i>

$PVC$	<i>Polyvinyl chloride</i>
$u_B$	<i>Bubble rising velocity (<math>m.s^{-1}</math>)</i>
$U_G$	<i>Gas superficial velocity (<math>m.s^{-1}</math>)</i>
$V_G$	<i>Gas volume (<math>m^3</math>)</i>
$VRF$	<i>virtual rheoscopic fluid</i>
$V_T$	<i>Total volume (<math>m^3</math>)</i>
$\varepsilon_G$	<i>Gas holdup</i>
$\varepsilon_S$	<i>Solid hold up</i>

640

641

642     **Table legends**

Table 1.	Physical packing characteristics (Garcia Maldonado, 2007)
Table 2.	Effect of superficial gas velocity on the volumetric mass transfer coefficient $k_L a$ for both types of packing
Table 3.	Evolution of hydrodynamics and mass transfer for different liquid phases ( $U_G = 0.0023 \text{ m/s}$ )
Table 4.	Bubble properties at local scale

643

644 **Figure legends**

Figure 1	Global scale experimental setup.
Figure 2	Local scale experimental setup
Figure 3	Principle of the colorimetric technique
Figure 5	Calibration procedure (a) Calibration curve between gray level and dissolved oxygen concentration (b) Variation of the gray level in the Hele-shaw cell for different resazurin concentrations
Figure 4	Image processing. (a) raw image (b) corrected image after subtraction of the background (c) corrected image after subtraction of the noise contribution (d) detection of the bubble contour (e) dissolved oxygen concentration field obtained after applying the calibration curve
Figure 6	Packing used at global scale (a) Meteor (b) Biolite P.3.5
Figure 7	Evolution of gas holdup (a) Gas holdup with all the compounds at $1\text{g.l}^{-1}$ for Meteor versus superficial gas velocity for Meteor (b) Comparison between gas hold up for clean water, NaCl ( $1\text{g.l}^{-1}$ ), glucose ( $1\text{g.l}^{-1}$ ), Acticarbon ( $1\text{g.l}^{-1}$ ) in Meteor and Biolite (c) Evolution of gas holdup with concentration ( $\text{g.l}^{-1}$ ) at superficial gas velocity of $0.0023\text{ m.s}^{-1}$
Figure 8	Evolution of interfacial area (a) with all the compounds at $1\text{g.l}^{-1}$ for Meteor versus superficial gas velocity for Meteor , (b) Comparison between interfacial area for clean water, NaCl ( $1\text{g.L}^{-1}$ ), glucose ( $1\text{g.L}^{-1}$ ), Acticarbon ( $1\text{g.L}^{-1}$ ) in Meteor and Biolite (c) Evolution of interfacial area with

	concentration ( $\text{g.L}^{-1}$ ) at superficial gas velocity of $0.0023\text{ms}^{-1}$
Figure 9	Evolution of volumetric mass transfer coefficient $k_{La}$ (a) with all the compounds at $1\text{g.l}^{-1}$ for Meteor versus superficial gas velocity for Meteor, (b) Comparison between volumetric mass transfer coefficient $k_{La}$ for Clean water, NaCl ( $1\text{g.L}^{-1}$ ), glucose ( $1\text{g.L}^{-1}$ ), Acticarbon ( $1\text{g.L}^{-1}$ ) in Meteor and Biolite (c) Evolution of volumetric mass transfer coefficient $k_{La}$ with concentration ( $\text{g.L}^{-1}$ ) at superficial gas velocity of $0.0023\text{m.s}^{-1}$
Figure 10	Visualization of bubble rise hydrodynamics by kalliросcopic technique (a) without packing (b) with packing
Figure 11	Visualization of hydrodynamics and oxygen transfer of bubble rising in Meteor (a) hydrodynamics visualization by kalliросcopic technique for bubble rising in Meteor (b) mass transfer visualization by colorimetric method for bubble rising in Meteor.
Figure 12	Visualization of hydrodynamics and oxygen transfer of bubble rising in Biolite (a) hydrodynamics visualization by Kalliросcopic technique for bubble rising in Biolite (b) mass transfer visualization by colorimetric method for bubble rising in Biolite
Figure 13	Mass transfer coefficient evolution with channel size for Meteor and Biolite packings

645

646

## References

- Andereck, C.D., Liu, S. S., Swinney, H. L., 1986. Flow regimes in a circular couette system with independently rotating cylinder, *Fluid Mechanic Journal* 4, 155–183.
- Asgharpour, M., Mehrnia, M-R., Mostoufi, N., 2010. Effect of surface contaminants on oxygen transfer in bubble column reactors, *Biochemical Engineering Journal*, 49, 351-360.
- Bhatia, B., Nigama, K.D.P., Aubanb, D., Hébrard, G., 2004. Effect of a new high porosity packing on hydrodynamics and mass transfer in bubble columns, *Chemical Engineering and Processing* 43 , 1371–1380.
- Chaudhary, D.S., Vigneswaran, S., Ngo, H.H., Shim, W.G., and Moon, H., 2003. Biofilter in Water and Wastewater Treatment, *Korean Journal of Chemical Engineering* 20(6), 1054-1065.
- Cook, A. G., Tolliver, R. M., Williams, J. E., 1994. The blue bottle experiment revisited gives some details of the reaction mechanism and alternative dyes. *J. Chem. Educ.* 71, 160.. DOI:10.1021/ed071p160
- Daeseong, J., Revankar, S.T., 2011. Investigation of bubble breakup and coalescence in a packed-bed reactor – Part 1:A comparative study of bubble breakup and coalescence models, *International Journal of Multiphase Flow* 37, 995–1002.
- Daeseong, J., Revankar, S.T., 2011. Investigation of bubble breakup and coalescence in a packed-bed reactor – Part 2: Development of a new bubble breakup and coalescence model, *International Journal of Multiphase Flow* 37, 1003–1012.
- Dumont, E., Andrès, Y., Le Cloirec, P., 2006. Effect of organic solvents on oxygen mass transfer in multiphase systems: Application to bioreactors in environmental protection, *Biochemical Engineering Journal* 30, 245–252.

671 Engerer, S.C, Gilbert Cook, A., 1999. The Blue Bottle Reaction as a General Chemistry  
 672 Experiment on Reaction Mechanisms. *J. Chem. Educ.* 76 (11), 1519. DOI:  
 673 10.1021/ed076p1519  
 674 Garcia Maldonado, J.G., Bastoul, D., Baig, S., Roustan, M., Hébrard, G., 2008. Effect of  
 675 solid characteristics on hydrodynamic and mass transfer in a fixed bed reactor operating  
 676 in co-current gas–liquid up flow, *Chemical Engineering and Processing* 47 , 1190–  
 677 1200.  
 678 Gullicks, H., Hasibul, H., Das, D., Moretti, C., and Yung-Tse Hung, Y.-T., 2011. Biofilm  
 679 Fixed Film Systems *Water* 3, 843-868.  
 680 Hébrard G. Etude de l'influence du distributeur de gaz sur l'hydrodynamique et le  
 681 transfert de matière gaz liquide des colonnes à bulles ; Thèse d'état , 1996.  
 682 Hikita, H., Kikukawa, H., 1974. Liquid phase mixing in bubble columns: effect of liquid  
 683 properties, *Chemical Engineering Journal* 8, 191-197.  
 684 Indrani, D., Grant Allen, D., 2005. Biofilter technology. *Biotechnology for Odor and Air*  
 685 *Pollution Control*, 125-146.  
 686 Jamnongwong, M., Loubiere, K., Dietrich, N., Hébrard, G., 2010. Experimental study of  
 687 oxygen diffusion coefficients in clean water containing salt, glucose or surfactant:  
 688 Consequences on the liquid-side mass transfer coefficients, *Chemical Engineering*  
 689 *Journal* 165, 758–768.  
 690 Lopez-Lopez, J.-S., Benbelkacem, H., Debellefontaine, H., 2007. Influence of *t*-butanol  
 691 and of pH on hydrodynamic and mass transfer parameters in an ozonation process,  
 692 *Chemical Engineering and Processing* 46 649–655.  
 693 Matisse, P., Gorman, M., 1984. Neutrally buoyant anisotropic particles for flow  
 694 visualization, *Physics of Fluids*, 27(4):759–760.

695 Moustiri, S., Hebrard, G., Roustan, M., 2002. Effect of a new high porosity packing on  
 696 hydrodynamics of bubble columns , *Chemical Engineering and Processing* , 41, 419-  
 697 426.

698 O'Brien J., Wilson, I., Orton, T., Pognan, F., 2000, Investigation of the Alamar Blue  
 699 (resazurin) fluorescent dye for the assessment of mammalian cell cytotoxicity, *Eur. J.*  
 700 *Biochem.* 267, 5421-5426

701 Omota, F., Dimian, A.C., Bliet, A., 2006. Adhesion of solid particles to gas bubbles. Part  
 702 1: Modeling, *Chemical Engineering Science* 61, 823 – 834.

703 Omota, F., Dimian, A.C., Bliet, A., 2006. Adhesion of solid particles to gas bubbles. Part  
 704 2: Experimental, *Chemical Engineering Science* 61, 835 – 844.

705 Plais, C., Billet, A.-M., Carine, J.-L., Delmas, H., 2005. Etude du transfert gaz-liquide en  
 706 présence d'une troisième phase finement divisées, *Récents Progrès en Génie des*  
 707 *Procédés* 92.

708 Roudet, M., Loubière, K., Gourdon, C., Cabassud, M., 2011, Hydrodynamics and mass  
 709 transfer in inertial gas-liquid flow regimes through straight and meandering  
 710 millimetric square channels, *Chem. Eng. Sci.* 66 2974-2990.

711 Stemmet, C.P., Bartelds, F., van der Schaaf, J., Kuster, B.F.M., Schouten, J.C., 2008.  
 712 Influence of liquid viscosity and surface tension on the gas–liquid mass transfer  
 713 coefficient for solid foam packings in co-current two-phase flow chemical engineering  
 714 research and design 86, 1094–1106.

715 Sundararajan, A., Ju, L.-K., 1993. Biological oxygen transfer enhancement in bioreactors,  
 716 *Trans IChemE* 71 , 221–223.

717 Walter R. Vandaveer, I.V., Mel Mosher, 1997. The blue bottle revisited. *J. Chem. Educ.*  
 718 74 (4), 402.. DOI: 10.1021/ed074p402.

719 Wellman, W. E., Noble, M.A., 2003. Greening the Blue Bottle. *J. Chem. Educ.* 80 (5),  
 720 537,. DOI: 10.1021/ed080p537.



721 Yue, J., Chen, G., Yuan, Q., Luo, L., Gonthier, Y., 2007. Hydrodynamics and mass  
722 transfer characteristics in gas–liquid flow through a rectangular microchannel. *Chem.*  
723 *Eng. Sci.* 62, 2096–2108.

724

725

726